BUNSEN-MAGAZIN · 16. JAHRGANG · 4/2014

Marcus Scheele

BRIDGING THE GAP: WHERE INORGANIC QUANTUM DOTS AND ORGANIC SEMICONDUCTORS MEET

1. INTRODUCTION

Inorganic semiconductor quantum dots (QD) are an emerging material class for optoelectronic applications. Mobilities as large as 35 $cm^2/V{\cdot}s$, carrier diffusion lengths of several hundred nanometers, low excitonic binding energies, size-tunable bandgaps and strong resistance to photo-bleaching have paved the way to successful implementation in solar cells, light-emitting diodes, photodetectors and field-effect transistors.[1–3] During the same period, organic semiconductors (OSC) have been at least equally successful in their application for optoelectronic devices.[4] High material purity, a large degree of crystalline ordering in thin films, well-defined spin-states and the capability for controlled doping render OSCs particularly suitable for application in transistors and light-emitting devices, where they are already used commercially. Interdisciplinary interactions between the two fields have been limited despite the possible synergism that arises by combining the advantageous properties of the two material classes. Looking through the eyes of an inorganic QD chemist, there is indeed a gap to be bridged, not only between two adjacent QDs separated by their often insulating ligand sphere, but also between the fields of QD and OSC research. I will argue that this gap may be overcome by utilizing OSC small molecules as surface ligands for inorganic QDs.

2. BASIC PRINCIPLES/CONCEPTS

The basic principles of electric transport through an array of close-packed QDs have been subject to a number of excellent reviews, far more comprehensive than the scope of this article would allow.[5,6,21] Briefly, the behavior of these artificial solids can be described as a network of spatially and energetically disordered hopping sites, where the mobility is determined by an interplay between electronic coupling, charging energy and energetic polydispersity.[44] This description of QD electronics is largely shared by the field of OSC electronics, but the two communities diverge greatly in their approach of the problem. Where continuous progress in the crystallization of OSCs has led to an ever-growing size of the average crystalline domain and therefore a reduction of hopping events, QD electronics is inherently based on small crystalline domains and a large number of hops. Where organic electronics aims to reduce the number of these detrimental hopping events, QD electronics is forced to make each hop less detrimental. The common strategies include increasing the particle-particle coupling strength, decreasing the charging energy and disorder, or a combination of these approaches.

2.1 ENERGETIC, ORIENTATIONAL AND SUPERLATTICE DISORDER

After 25 years of research, the size distribution of the most advanced QDs is now 4 %.[7] Despite this remarkable development, 4 % translates to a standard deviation of roughly 150 atoms per individual QD (assuming a spherical QD of ~1000 atoms). In light of the much celebrated property-size relationship for QDs in the strong quantum confinement regime, this variance is still very significant. Following a recent argument by Guyot-Sionnest, it is equivalent to an energy dispersion of ~25 meV for a typical QD with a confinement energy of 0.5 eV and, thus, to kT at room temperature.[44] A carrier travelling across an array of QDs with this energetic polydispersity should be greatly affected by the fluctuations in energy level positions and the offsets in between.

Therefore, it is puzzling that attempts to quantify the effect of energetic disorder on transport through a QD array have revealed at most a weak dependence.[22] Further, a QD sample with a bimodal size-distribution has been found to exhibit transport properties expected for a monomodal sample of the more conductive particle species. These findings underline the importance of percolative pathways, which form in an array of polydisperse QDs and possibly even out most of the effects of energetic polydispersity. This effect may be visualized by imagining a QD array as an ensemble of 1D- channels of individual QDs connecting the source and drain electrode. Where the QDs of each channel are connected in series, the 1D-channels contribute to the total resistance of the array like resistors in a parallel circuit. A reasonably narrow size-distribution provided, there will always be enough QDs of very similar size to exceed the so-called percolation threshold and form a coherent channel.[8] The total resistance of the array is dominated by this channel and the contribution of the less efficient channels with

Dr. Marcus Scheele
Eberhard Karls Universität Tübingen
Faculty of Science, Institute of Physical and Theoretical Chemistry
Auf der Morgenstelle 18, 72076 Tübingen, Germany
Phone: +49 7071 29-76243
E-Mail: marcus.scheele@uni-tuebingen.de

larger energetic polydispersity remains weak. This important difference to single-channel devices is sometimes neglected when estimating the effect of site disorder for QD electronics.

Nonetheless, future improvements in the controlled synthesis and assembly to arrays of QDs will certainly have a positive impact on their transport properties. Particularly relevant to this prediction is another type of disorder, which I refer to as "orientational disorder". QD-based devices undergo a dramatic improvement in carrier transport if the individual particles show preferential alignment along a shared crystal axis.[9] Such alignment can be achieved, for instance, by exploiting the rich shape control in QD synthesis which leads to a preferential orientation in close-packed arrays. A remarkable computational study on PbSe QDs revealed that the spatial orientation of QD wave functions varies with the shape, that is, the ratio of (001) to (111) facets.[32] In a cubic system like PbSe, the two extremes in this respect are the cube and the octahedron. According to the results of this study, the hole ground state ($1S_h$) will extend preferentially in the direction of the facet with the largest area, whereas the electron ground state ($1S_e$) does the opposite. This means that for a close-packed array of cubes, hole transport is greatly favored over electron transport since cubes tend to align in the [001] direction. For a chain of octahedra with tip-to-tip connections (also along the [001] direction), electron transport should be favored. It would be very exciting to see the predictions of this computational model supported by appropriately designed experiments. The necessary chemical protocols are already available.[10]

A similar type of disorder is "superlattice disorder". Inspired by the pioneering work of Shevchenko *et al.*, the potential of nanocrystals with narrow size-distribution to display quasi-atomic behavior and self-assembly into crystal-like superlattices has been explored, described theoretically and exploited for device applications by several groups.[11,12,51,54] Although improved transport in self-assembled QD arrays unambiguously related to a high degree of superlattice order has not been demonstrated yet, the potential for miniband formation in highly ordered QD arrays renders superlattice disorder potentially important for carrier transport as well.[13] For practically uniform QDs fabricated by molecular beam epitaxy, this effect was observed decades ago.[14]

In conclusion, disorder in QD arrays needs to be minimized in order to optimize carrier transport. This can be achieved by further narrowing the size-distribution and/or controlling the QD shape and their assembly into superlattices. However, some types of disorder may have a more dramatic effect onto transport through a QD array than others, and a combined assessment – experimentally as well as theoretically – of these differences could be very rewarding in order to advance the field.

2.2 CHARGING ENERGY TO CARRIER INJECTION

The charging energy of a single nanoparticle corresponds to the energy required to place an additional charge on that particle. According to the modified Laikhtman-Wolf model, it is given by the self-capacitance (C_s) of the particle and the mutual capacitance (C_M) between it and its neighbors,

$$E_c = \frac{e^2}{2(C_s + nC_M)}$$

where *e* is the elemental charge and *n* is the average number of nearest neighbours.[15] The self-capacitance of a spherical nanoparticle with a static dielectric constant (ε_{np}) and surrounded by a ligand matrix of static dielectric constant (ε_m), is given by,

$$C_s^{-1} = \frac{1}{4\pi\epsilon_0 r}\left(\frac{\epsilon_{np}-\epsilon_m}{\epsilon_{np}\epsilon_m}\right) + \frac{0.94}{4\pi\epsilon_{np}\epsilon_0 r}\left(\frac{\epsilon_{np}-\epsilon_m}{\epsilon_{np}+\epsilon_m}\right)$$

where *r* is the nanoparticle radius.[16] Due to the size-dependence of the oscillator strength in quantum-confined crystallites, ε_{np} is often found to exhibit a significant size-dependence as well. This can be accounted for by applying a generalized Penn Model,[17,18]

$$\epsilon_{penn} = 1 + \frac{\epsilon_{bulk} - 1}{1 + \frac{18.05}{r^{1.8}}}$$

where *r* is the nanoparticle radius in nanometers. Likewise, the mutual capacitance is given by,

$$C_M = 2\pi\epsilon_0\left(\frac{\epsilon_{np}\epsilon_m}{\epsilon_{np}-\epsilon_m}\right) r\, ln\left(\frac{2r+s}{s}\right)$$

where s is the edge-edge nanoparticle spacing.[22]

It follows that the charging energy of a given QD material decreases by a) increasing the nanoparticle diameter, b) increasing the packing density of the QD solid, c) increasing the static dielectric constant of the ligand sphere or d) decreasing the interparticle spacing. I stress here that particularly the last two parameters are manipulated substantially upon applying some of the recently very popular "short ligand exchange" strategies.[19,52,53] Despite the unarguable success of these protocols to yield conductive QD films, it is surprising how quickly the improved transport properties of such films are often attributed to increased coupling. They may also result (in part) from decreased charging energies.

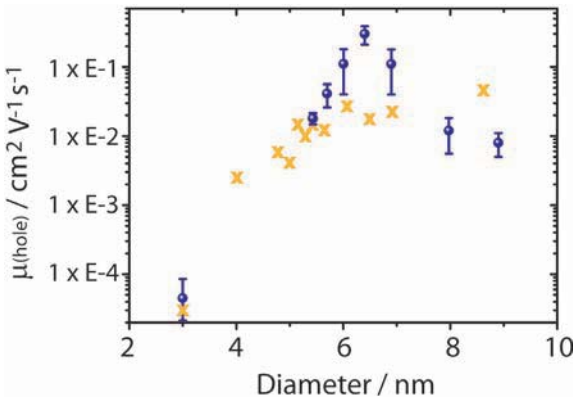

Fig. 1: Size-dependent field-effect hole mobilities of PbSe QD solid films. (Blue circles) Particles capped with Pb(methoxide)$_2$ show a nonmonotonic size dependence indicative of a comparable magnitude of coupling and charging energy. Error bars are standard deviations from at least three different devices. (Orange crosses) In contrast, particles capped with Pb(ethanedithiolate) reveal a monotonic mobility increase with QD size which indicates the dominant effect of charging effects and overall smaller coupling energies. Reprinted with permission from reference 27. Copyright 2013. American Chemical Society.

2.3 PARTICLE-PARTICLE COUPLING

According to the Miller-Abrahams expression, electronic coupling in QD arrays scales with exp(-βd), where d is the interparticle spacing and β is a constant that depends on the carrier effective mass as well as the height of the tunneling barrier, and provides a measure for the leakage of the wave function.[20,21] Since the latter monotonically decreases with increasing QD size, particle-particle coupling under otherwise identical conditions is generally larger for smaller QDs. As this is the opposite trend to the size-dependence of the charging energy, interesting phenomena like maxima in the size-dependence of carrier mobilities can occur if charging and coupling energies are of comparable magnitude (see Fig. 1).[22,27] This raises the question of how large coupling in typical QD solids actually is and how it can be measured. One simplifying approach is to use the carrier mobility (μ) and extrapolate the coupling energy (V) by applying the Einstein-Smoluchowski relationship:

$$\mu = \frac{e(d^2)V}{2\hbar k_b T}$$

where *e* is the elemental charge, *d* the interparticle spacing, *h* Planck's constant, k_b Boltzmann's constant and *T* the absolute temperature. However, this estimate is only useful if coupling is much greater than the effect of disorder or the charging energy since the Einstein-Smoluchovski relationship does not include the latter effects. For common QD solids, coupling and charging energy are of comparable magnitude as discussed above, such that this method is hardly reliable: For a QD solid with mobilities on the order of 10^{-2} cm^2/V-s, coupling energies between 8 μeV and 10 meV have been calculated.[23,44]

Another popular measure for particle-particle coupling mediated by a certain ligand system is to investigate the optical shift of the first excitonic transition upon ligand exchange of a highly insulating ligand sphere with the molecule in question. This measure is very convenient and unaffected by charging effects due to open-circuit conditions. Bathochromic shifts of up to 220 meV have been observed and the size-dependence followed the expected trend for coupling by increasing with decreasing diameter.[27,41] However, this technique requires careful treatment of the impact by the ligand exchange on the dipole-dipole interactions in the QD film.[24] In 2001, Döllefeld *et al.* observed a 29 meV bathochromic shift for CdS clusters upon assembly into compact films from solution.[25] Using a simple dipole-dipole model, the authors could attribute the shift entirely to dielectric effects with virtually no contribution from coupling. According to this model, the incoming electromagnetic field induces dipoles in neighboring particles that change the average field and reduces the dipole transition energy by,

$$E_{dipole-dipole} = \frac{\mu_{tr}^2 \alpha}{\pi \epsilon_0} D^{-6}$$

where μ_{tr} is the transition dipole moment, α is the polarizability volume, ε_0 is permittivity of free space, and *D* is the particle-particle distance. The transition dipole moment,

$$\mu_{tr} = \sqrt{\frac{3he^2}{8\pi^2 m_e \nu_{max}} f}$$

depends both on ν_{max}, the wavenumber of the first exciton peak, and *f*, the oscillator strength of the corresponding transition. Although the size-dependence of the polarizability has recently been shown to approach the bulk value for clusters as small as 30 atoms,[26] ν_{max} and therefore μ_{tr} are strongly size-dependent for typical QDs, such that dipole-dipole interactions are usually increasing with decreasing QD size.[27] Because this is the same trend as expected for electronic coupling, size-dependent bathochroism is an ambiguous measure for the coupling strength in QD ensembles and needs to be interpreted with care.

Since then, several groups have conducted similar experiments – mainly on PbSe QDs – and arrived at comparable conclusions: The bathochromic shift observed so far in common QD solids upon ligand exchange, accompanied by a notable increase in conductivity, is almost completely due to dipole-dipole interactions and *not* a signature of particle-particle coupling.[27,28,52] Amongst the quickly growing number of reports on improving transport in QD solids, the advent of a bathochromic shift in this context is sometimes still quickly interpreted as an unambiguous indication of improved coupling. This should be viewed with skepticism.

Coupling in close-packed QDs (Si, PbSe and InAs) has also been measured by scanning tunneling spectroscopy.[29–31] The results vary greatly – even on the same material system – between 10 meV and 330 meV indicating that, despite the elegance of this method, there may be additional effects to be considered which can bias the determination of the coupling strength.

Finally, the coupling strength between PbSe QDs of different shapes and diameters around 2 nm has been calculated with density functional theory.[32] For an interparticle spacing of 0.5 nm, coupling varied between 1 and 50 meV depending on whether hole or electron transport was considered and along which crystalline direction it occurred. This highlights the great complexity of controlling the coupling energy in QD ensembles.

To conclude, a precise determination of the coupling strength in QD solids is complex and requires further refinements of existing methods. A theory which unifies the combined effects of disorder, charging energy and coupling onto the carrier mobility in QD solids would be greatly desirable. The coupling energy in state-of-the-art QD solids appears to be on the order of the charging energy. The prospects of a QD material with coupling energies that significantly exceed the charging energy and the goal of *band-like transport* has motivated the search for new concepts to improve particle-particle interactions. Fundamentally, this aim requires a reduction of either the width or the height of the barrier to carrier transport.

3. THE CONCEPT OF COUPLED ORGANIC-INORGANIC NANOSTRUCTURES (COIN)

3.1 DEFINITION

Most colloidal nanoparticles consist of an inorganic core – the "particle" – and an organic shell – the "ligands".[33] Many methods have been developed to manipulate the ligand shell and

utilize the electronic interactions between particle and ligand to tailor the properties of the whole structure. Exchange with organic molecules of similar backbone but different functional group, with much smaller length, and with thermally labile organic molecules designed to result in virtually bare nanoparticles after thermolysis have been reported.[34,37,52] There has also been great interest in the properties of blended hybrid materials obtained by intimate mixing of nanoparticles with organic moieties, usually polymers.[35] If both materials are semiconductors, interesting synergetic properties can arise which have been recently reviewed by Agranovich *et al*.[36] None of the above will be referred to as COINs in this article. In contrast, a COIN is composed of a semiconducting inorganic nanoparticle – a quantum dot (QD) – and an organic semiconductor (OSC) *covalently coupled* to the surface of the QD.

3.2 OPTICAL PROPERTIES

Charge-carrier transfer between a nanoparticle and chemisorbed ligands is commonly observed also for nanoparticle systems with insulating ligands. For example, alkanethiols attached to the surface of cadmium chalcogenide QDs are efficient hole receptors.[37] Chalcogenidometalates bound to CdSe-CdS QDs have been shown to result in extremely long lifetimes for trapped holes.[38] The fluorescence quantum yield of these structures is greatly reduced due to localized charges in the QD after charge transfer into the ligand sphere. Fast and non-radiative Auger processes occur efficiently in charged emitters such that the QD remains mostly in the poorly emitting off-state.[39] When the accepting ligand is removed and the charge transfer pathway blocked, the emitter returns into the brightly fluorescent on-state.[40]

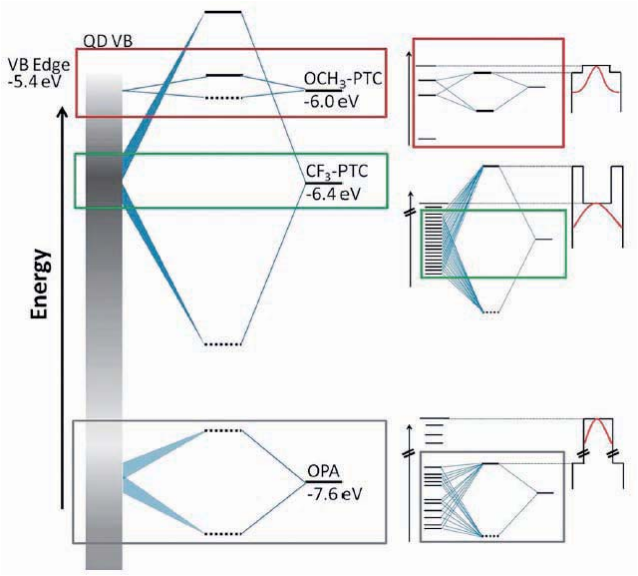

Fig. 2: (left) Schematic representation of the energetic alignment and splitting of orbitals of the CdSe hole states (represented by the gray bar, where higher density of states is darker) and three ligands: the native ligand octylphosphonate (OPA) as well as the two phenyldithiocarbamates CF_3-PTC, and OCH_3-PTC. (right) Zoomed-in views of the hybridized orbitals created by mixing of hole states with the HOMO of each ligand and the corresponding diagram for the confining potential for the excitonic hole (wave function sketched in red) resulting from these hybridized orbitals. The potential profile is defined by the $1S_h$ state and the hybridized HOMO. The particle-in-a box diagrams are "upside-down" because the profiles are for holes, not electrons. Reprinted with permission from reference 41. Copyright 2012. American Chemical Society.

These transfer events from the QD to the ligand rely on either a highest occupied molecular orbital (HOMO) at or above the hole ground state (1Sh) in the QD or a lowest unoccupied molecular orbital (LUMO) at or below the QD electron ground state ($1S_e$). Because the ligand in COINs by definition contains a HOMO-LUMO gap of similar magnitude as the $1S_h$-$1S_e$ gap in the QD, this precondition is usually met in COINs. Frederick et al. have presented an exciting example of CdSe QDs passivated with phenyldithiocarbamates (PTC).[41,42] PTCs are wide-gap semiconductors with HOMOs (~ -6.0 eV) slightly below the $1S_h$ state in CdSe QDs (~ -5.5 eV). Upon ligand exchange from the native octylphosphonate ligand to PTC, a bathochromic shift of up to 220 meV is observed. Decreasing the electron-withdrawing nature of the substituents on the aromatic ring decreases the magnitude of the shift. This effect is attributed to 1) efficient mixing of the HOMO with a region of high density of states (DOS) inside the valence band of CdSe and 2) energy level alignment between the $1S_h$ state of the QD and the hybridized, interfacial state obtained by orbital mixing between $1S_h$ and HOMO of lowest energy for holes. The authors argue that because of the former precondition, a ligand with a HOMO positioned significantly below the $1S_h$ state can still lead to larger hole delocalization compared to a similar ligand with a HOMO in close energetic proximity to the $1S_h$ state (see Fig. 2). This is the consequence of the reduced DOS in a QD close to the $1S_h$ state compared to regions somewhat deeper inside the valence band. The latter precondition is used to explain why ligands with very low lying HOMOs do not result in large bathochromic shifts despite their mixing with a region of presumably large DOS: The energetic splitting upon orbital mixing must overcome the initial energy offset between $1S_h$ state and the HOMO. If this offset is very large (2.2 eV in the case of octylphosphonate), even significant splitting of the hybridized interfacial orbitals will not be sufficient to close the gap and the delocalization of holes remains weak. Although some of the conclusions made by the authors should be reviewed carefully in the light of section 2.3, the observed optical shift is so significant that a coupling component despite the inevitable dipolar effects upon ligand exchange seems plausible.

The next step in exploring and exploiting this novel concept for coupling between a QD and its ligand sphere is to expand the system from an isolated COIN to an ensemble of COINs in intimate contact. This provides the possibility to probe the coupling not only *via* the optical properties but also in terms of electrical transport and real particle-particle coupling mediated by the OSC ligand shell.

3.3 ELECTRICAL PROPERTIES OF COIN ENSEMBLES

As demonstrated in the last section, organic molecules with appropriately positioned HOMO or LUMO levels are theoretically suited to establish resonant tunneling with the 1S states in QDs. For Au nanoparticles functionalized with partially conjugated dithiocarbamates, this result has been demonstrated by varying the number of non-conjugated bonds within the ligand.[43] It was shown that carrier transport depends exponentially on the number of non-conjugated bonds as predicted by the Miller-Abrahams expression (see section 2.3) and that tunneling through conjugated bonds is resonant.

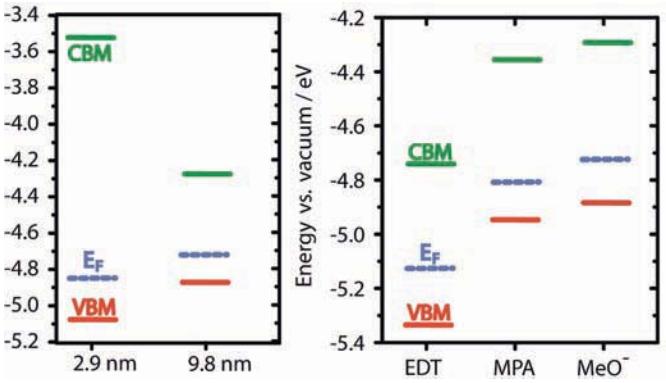

Fig. 3: Fermi level, valence band maximum (VBM) and conduction band minimum (CBM) values of PbS nanoparticles with different diameter and methoxide capping (left) as well as different ligands – namely ethanedithiol (EDT), mercaptopropionic acid (MPA) and methoxide (MeO) - and 9.8 nm diameter (right). Dashed lines show the measured Fermi level and full lines indicate the calculated VBM (red) and CBM (green). Note that for strongly confined QDs, the terms VBM and CBM are synonyms for the $1S_h$ and $1S_e$ state, respectively. Reprinted with permission from reference 48. Copyright 2013. American Chemical Society.

As Guyot-Sionnest has pointed out, there is no reason why the same concept should not work for semiconductor QDs as well, except that its realization may be more challenging:[44] The DOS in metals near the Fermi level is usually large and many channels for resonant tunneling into a bound ligand are available. In semiconductor QDs however, the DOS is much smaller and the number of channels may be limited to just one. (The degeneracy of the 1S states in some materials can slightly increase this number; e.g. PbSe: degeneracy = 4, number of channels = 16). It is then of paramount importance to tune the position of the $1S_h$ ($1S_e$) state in the QD such that it comes into resonant alignment with the hybridized HOMO (LUMO) of the OSC. Fortunately, the size-dependence of the absolute energy of the 1S states in QDs provides a powerful tool to realize such tuning *via* synthetic control of the QD diameter. An ensemble of energy level aligned COINs can be viewed as a connection of QD resistors which are electronically coupled through their OSC ligand shells. Transport in this system occurs along percolative pathways of repetitive double-barrier tunnel junction units where the two barriers are of identical magnitude (assuming fully monodisperse QDs) but opposite sign. For this reason and in contrast to the optical experiments described by Frederick *et al.,* any potential difference between the QD and OSC – negative or positive – needs to be minimized by near-resonant energy level alignment in order to achieve large in-film carrier mobilities. Unless the HOMO-LUMO gap of the OSC is the same as the $1S_h$-$1S_e$ gap (the "bandgap") of the QD, the alignment is necessarily limited to one carrier. This gives access to QD films which are carrier-specific in their transport behavior without the need to control the doping concentration. A first example of such a system are thin films of PbS QDs cross-linked with tetrathiafulvalene tetracarboxylate (TTFTA).[55] Tetrathiafulvalene derivatives are well-studied OSCs with HOMO-LUMO gaps of 2.5 – 3.0 eV with excellent electron-donating properties, a fully conjugated, non-aromatic π-system and a HOMO positioned between -4.5 and -5.0 eV against vacuum.[45] PbS QDs on the other hand combine a large tunability of the $1S_h$-$1S_e$ gap over a range of > 1.0 eV with high static dielectric constants (size-dependent; usually around 18). The latter leads to low charging energies, which facilitates carrier transport as demonstrated in section 2.2. The size-dependence of the absolute energies of the 1S states (particularly the hole state) have also been thoroughly investigated.[46,47] Using gas-phase core-level X-ray photoelectron spectroscopy, the dependence of the $1S_h$ energy in PbS QDs on the chemical nature of the ligand binding to the surface of the QD has been revealed (see Fig. 3).[48] I stress that the consequences for the interfacial electronic structure on the interaction between the OSC and QD are easily underestimated. To this end, there is still much to learn from the well-developed field of molecular monolayer interactions on bulk surfaces, for which insightful rationales have already been developed.[49] With this is mind, one can use the position of the 1S state in *isolated* QDs and compare it with the MO energy in the *isolated* OSC to approximate the energy alignment and barrier height for carriers in a covalently bound QD/OSC *hybrid*, that is, a COIN.

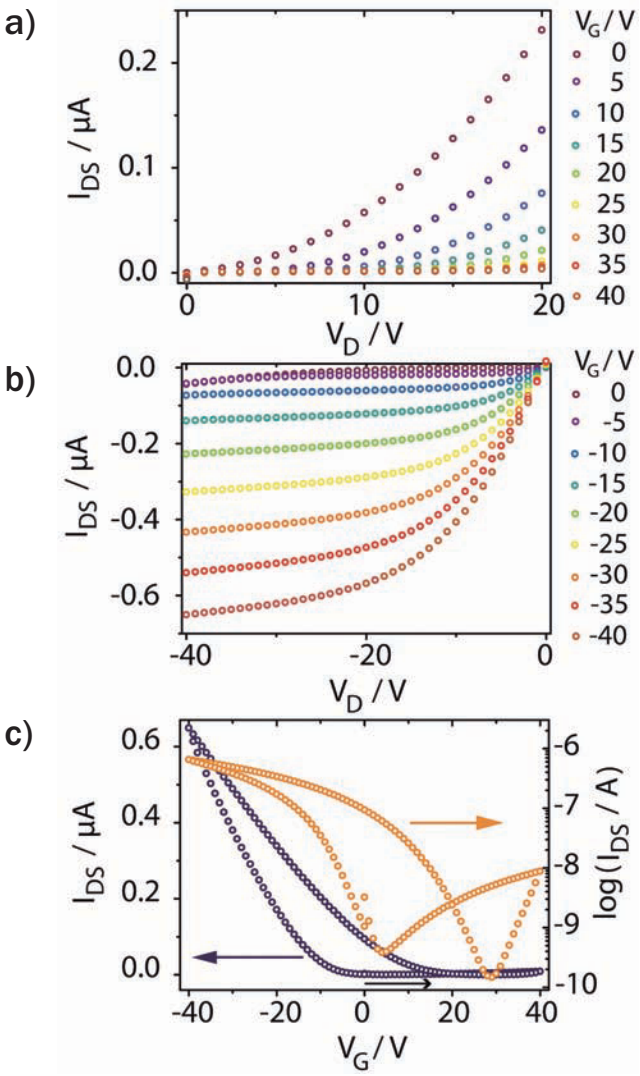

Fig. 4: Field-effect transistor characteristics of thin films of 9.8 nm PbS-TTFTA. (a,b) display positive and negative source-drain sweeps, with the applied gate voltages (V_G) for an individual sweep denoted next to each color. I_{DS} and V_D = current and potential difference between source and drain electrodes, respectively. (c) Transconductance under a constant V_D bias of +5 V. Left and right axes are linear and logarithmic plots of the same measurement, respectively. The black arrow indicates begin and direction of the closed loop scan. Reprinted with permission from reference 55. Copyright 2014. American Chemical Society.

In the aforementioned example of PbS QDs functionalized with TTFTA, near-resonant alignment between the organic HOMO and the inorganic 1Sh state was predicted in contrast to a large energetic difference between the LUMO and the $1S_e$ state. Therefore, one would expect preferential hole conduction and strongly inhibited electron conduction, which is indeed supported by field-effect transistor measurements (see Figure 4): Transport is p-type with only a weak contribution by electrons. The transconductance scan (Fig. 4c) reveals much larger carrier flows for negative gate voltages than for positive values, indicative of a visible preference for hole over electron transport.

It is also worth mentioning that a blend of PbS QDs and tetrathiafulvalene (without direct surface functionalization) exhibits size-dependent photoluminescence quenching.[50] This result suggests that the $1S_h$ state and the hybridized, interfacial HOMO in this system are close enough such that the potential difference can be tuned from negative through zero to positive upon varying the QD diameter. It will be intriguing to see if a similar size-dependence can also be found in the transport properties of the PbS QDs functionalized with TTFTA and how sharp the resonance in the field-effect mobility is upon finding the optimized QD size.

Bearing in mind that this concept is still in its infancy and substantial further development is required, in principle, very large coupling energies should be possible with the COIN approach since there are no lower-bound limitations to the height of the tunneling barrier. For an optimized system, the limiting factor for transport in the COIN film will be disorder as described in 2.1 and not, as is currently the case, interparticle coupling. To this end, COINs also bear advantages in terms of the structural properties over the state-of-the-art "short ligand strategies" (SLS) which are commonly used to build conductive QD films.[52]

3.4 STRUCTURAL PROPERTIES OF COIN ENSEMBLES

If the size distribution of a colloidal QD sample is sufficiently narrow, crystal-like long-range order in films on a substrate can be achieved.[51] For QD/ligand combinations which do not form stable colloids, a two-step approach is applied for self-assembly:[52] At first, the QDs are stabilized in solution utilizing a long-chained monodendate ligand (e.g. oleic acid, octadecylphosphonic acid, *etc.*) and self-assembled into a superlattice, followed by exchange on the substrate with the new ligand of choice. However, when such a superlattice of nanoparticles functionalized with a long-chained hydrocarbon is treated with a ligand of shorter length, strain is imposed onto the network due to the length difference between old and new ligand which destroys the superlattice.[52,53] This is an inherent disadvantage of the commonly applied SLS, which aims precisely at reducing the interparticle spacing to decrease the tunneling barrier width and increase particle-particle coupling. Another hindering factor in maintaining QD order is the short interparticle spacing itself. As Wang *et al.* have shown, the formation of QD superlattices can be expressed in an interparticle distance-dependent phase diagram requiring a certain minimal distance to enter the regime of stable superattices.[54] In the case of PbS QDs, this threshold distance is approximately 1.8 nm which is significantly above the interparticle distances imposed by SLS (0.1 – 0.3 nm).

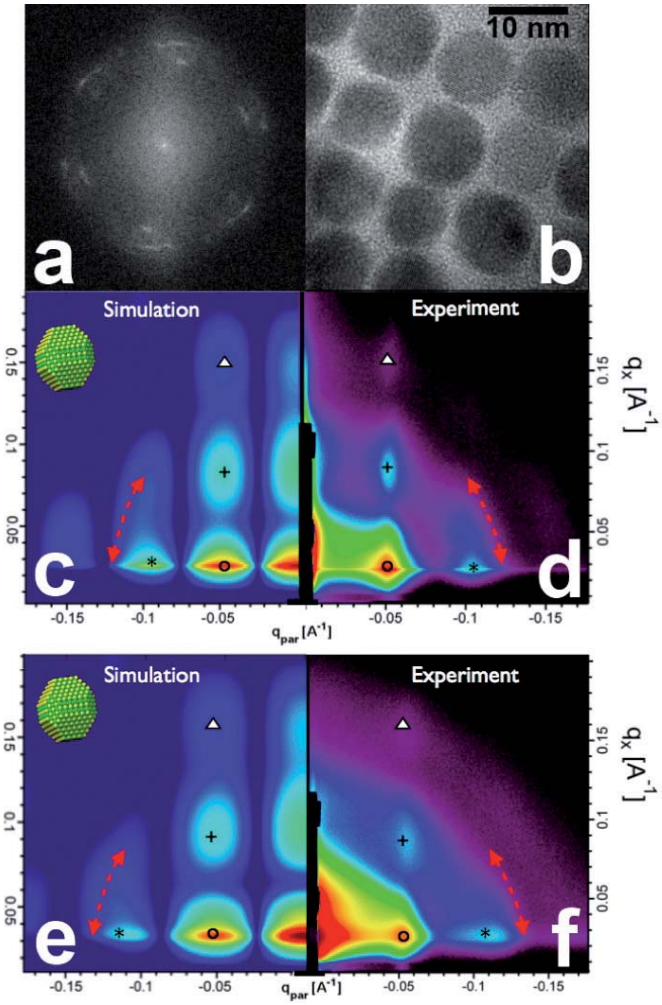

Fig. 5. (a) Fast Fourier transformation of a low magnification electron microscopy image of a PbS-TTFTA nanoparticle thin film. (b) Transmission electron microscopy image of self-assembled PbS-TTFTA nanoparticles. (c-f) Simulation and experimental Grazing-Incidence Small-Angle X-Ray Scattering images (left and right panel respectively) for PbS-Oleate (c,d) and PbS-TTFTA (e,f) thin films. Corresponding peaks are indicated by the same symbol. Red arrows are a guidance to the eye to underline the curvature of the scattering signal, which is indicative of a rhombicuboctahedral particle shape. q_{par} and q_x are the scattering signals parallel and perpendicular to the substrate surface. Reprinted with permission from reference 55. Copyright 2014. American Chemical Society.

In contrast, COINs do not have length constraints and fully conjugated OSCs with a molecular length > 1.8 nm are readily available. Due to the structural rigidity of the sp^2-carbon backbone in OSCs, the interparticle spacing is simply the length of the OSC. This has been demonstrated for the PbS-TTFTA system, where an interparticle spacing of roughly 10 Å has been found in accordance with a length of 9.6 Å for TTFTA.[55] It is presumably this greater length compatibility with the native ligand that leads to the observed partial preservation of structural order in superlattices of PbS QDs after exchange with TTFTA (see Fig. 5): Upon comparing corresponding peaks (denoted by the same symbol) before and after ligand exchange, a shift to slightly larger values of q_{par} is found which translates into a contraction of the interparticle spacing. However since this

contraction is relatively small compared to the shifts obtained by common SLS approaches, the scattering shape is largely preserved, and the absence of ring-like features indicates a significant degree of structural order. One can speculate that an even longer OSC with perfect length compatibility to the native ligand and interparticle spacings > 1.8 nm could lead to electronically coupled superlattices with long-range order.

4. OUTLOOK

Coupled organic-inorganic nanostructures (COIN) provide a different approach towards the realization of strongly coupled semiconductor quantum dot films. The advantages are highly tunable and carrier-specific coupling energies, the prospect of resonant tunneling and the formation of superlattices with low structural disorder. Where these properties are unrivaled by other existing strategies to bridge the gap between adjacent quantum dots in an electric circuit, the concept is certainly still in its infancy and requires an in-depth exploration as well as the development of new material combinations. To this end, much can be learned from the field of organic semiconductors, be it the understanding of electronic interactions of molecules covalently coupled to quantum dot surfaces, or the choice of suitable ligands.

5. ACKNOWLEDGEMENTS

Financial support of this work has been provided in equal parts by the Institutional Strategy of the University of Tübingen (Deutsche Forschungsgemeinschaft, ZUK 63) and the Baden-Württemberg Stiftung by the Eliteprogram for Postdocs. The PbS-TTFTA system was developed in the laboratories and under the guidance of A. Paul Alivisatos. The idea to use TTFTA as a covalent linker for coupled quantum dots was originally brought up by Yi Liu. I am grateful to David K. Britt and Jannika Lauth for a critical review of the manuscript.

6. BIBLIOGRAPHY

[1] Chung, D. S.; Lee, J.-S.; Huang, J.; Nag, A.; Ithurria, S.; Talapin, D. V. Low Voltage, Hysteresis Free, and High Mobility Transistors from All-Inorganic Colloidal Nanocrystals. *Nano Lett.* **12**, 2012, 1813–1820.

[2] Maraghechi, P.; Labelle, A. J.; Kirmani, A. R.; Lan, X.; Adachi, M. M.; Thon, S. M.; Hoogland, S.; Lee, A.; Ning, Z.; Fischer, A.; *et al.* The Donor-Supply Electrode Enhances Performance in Colloidal Quantum Dot Solar Cells. *ACS Nano* **7**, 2013, 6111–6116.

[3] Zhitomirsky, D.; Voznyy, O.; Hoogland, S.; Sargent, E. H. Measuring Charge Carrier Diffusion in Coupled Colloidal Quantum Dot Solids. *ACS Nano* **7**, 2013, 5282–5290.

[4] *Physics of Organic Semiconductors*; Brütting, W.; Adachi, C., Eds.; WILEY-VCH, 2012.

[5] Kim, J.-Y.; Kotov, N. A. Charge Transport Dilemma of Solution-Processed Nanomaterials. *Chem. Mater.* **26**, 2013, 134–152.

[6] Talapin, D. V.; Lee, J.-S.; Kovalenko, M. V.; Shevchenko, E. V. Prospects of Colloidal Nanocrystals for Electronic and Optoelectronic Applications. *Chem. Rev.* **110**, 2009, 389–458.

[7] Chen, O.; Zhao, J.; Chauhan, V. P.; Cui, J.; Wong, C.; Harris, D. K.; Wei, H.; Han, H.-S.; Fukumura, D.; Jain, R. K.; *et al.* Compact High-quality CdSe-CdS Core-Shell Nanocrystals with Narrow Emission Linewidths and Suppressed Blinking. *Nat Mater* **12**, 2013, 445–451.

[8] Mathew, M.; Schilling, T.; Oettel, M. Connectivity Percolation in Suspensions of Hard Platelets. *Phys. Rev. E* **85**, 2012, 061407–.

[9] Sun, B.; Sirringhaus, H. Solution-Processed Zinc Oxide Field-Effect Transistors Based on Self-Assembly of Colloidal Nanorods. *Nano Lett.* **5**, 2005, 2408–2413.

[10] Houtepen, A. J.; Koole, R.; Vanmaekelbergh, D.; Meeldijk, J.; Hickey, S. G. The Hidden Role of Acetate in the PbSe Nanocrystal Synthesis. *J. Am. Chem. Soc.* **128**, 2006, 6792–6793.

[11] Bodnarchuk, M. I.; Kovalenko, M. V.; Heiss, W.; Talapin, D. V. Energetic and Entropic Contributions to Self-Assembly of Binary Nanocrystal Superlattices: Temperature as the Structure-Directing Factor. *J. Am. Chem. Soc.* **132**, 2010, 11967–11977.

[12] Gomez-Grana, S.; Perez-Juste, J.; Alvarez-Puebla, R. A.; Guerrero-Martinez, A.; Liz-Marzan, L. M. Self-Assembly of Au@Ag Nanorods Mediated by Gemini Surfactants for Highly Efficient SERS-Active Supercrystals. *Advanced Optical Materials* **1**, 2013, 477–481.

[13] Lazarenkova, O. L.; Balandin, A. A. Miniband Formation in a Quantum Dot Crystal. *Journal of Applied Physics* **89**, 2001, 5509–5515.

[14] Esaki, L.; Chang, L. L. New Transport Phenomenon in a Semiconductor "Superlattice". *Phys. Rev. Lett.* **33**, 1974, 495–498.

[15] Quinn, A.; Beecher, P.; Iacopino, D.; Floyd, L.; De Marzi, G.; Shevchenko, E.; Weller, H.; Redmond, G. Manipulating the Charging Energy of Nanocrystal Arrays. *Small* **1**, 2005, 613–618.

[16] Lannoo, M.; Delerue, C.; Allan, G. Screening in Semiconductor Nanocrystallites and Its Consequences for Porous Silicon. *Phys. Rev. Lett.* **74**, 1995, 3415–3418.

[17] Penn, D. R. Wave-Number-Dependent Dielectric Function of Semiconductors. *Phys. Rev.* **128**, 1962, 2093–2097.

[18] Sharma, A. C. Size-dependent Energy Band Gap and Dielectric Constant Within the Generalized Penn Model Applied to a Semiconductor Nanocrystallite. *J. Appl. Phys.* **100**, 2006, 84301–8.

[19] Talapin, D. V.; Murray, C. B. PbSe Nanocrystal Solids for n- and p-Channel Thin Film Field-Effect Transistors. *Science* **310**, 2005, 86–89.

[20] Miller, A.; Abrahams, E. Impurity Conduction at Low Concentrations. *Phys. Rev.* **120**, 1960, 745–755.

[21] Remacle, F.; Levine, R. D. Quantum Dots as Chemical Building Blocks: Elementary Theoretical Considerations. *ChemPhysChem* **2**, 2001, 20–36.

[22] Liu, Y.; Gibbs, M.; Puthussery, J.; Gaik, S.; Ihly, R.; Hillhouse, H. W.; Law, M. Dependence of Carrier Mobility on Nanocrystal Size and Ligand Length in PbSe Nanocrystal Solids. *Nano Lett.* **10**, 2010, 1960–1969.

[23] Lee, J.; Choi, O.; Sim, E. Nonmonotonic Size-Dependent Carrier Mobility in PbSe Nanocrystal Arrays. *J. Phys. Chem. Lett.* **3**, 2012, 714–719.

[24] Foos, E. E. The Complex Interaction of Spectroscopic Shifts and Electronic Properties in Semiconductor Nanocrystal Films. *J. Phys. Chem. Lett.* **4**, 2013, 625–632.

[25] Doellefeld, H.; Weller, H.; Eychmueller, A. Particle-Particle Interactions in Semiconductor Nanocrystal Assemblies. *Nano Lett.* **1**, 2001, 267–269.

[26] Goetz, D. A.; Heiles, S.; Schaefer, R. Polarizabilities of SiN (N = 8-75) Clusters from Molecular Beam Electric Deflection Experiments. *The European Physical Journal D* **66**, 2012, 1–4.

[27] Scheele, M.; Engel, J. H.; Ferry, V. E.; Hanifi, D.; Liu, Y.; Alivisatos, A. P. Nonmonotonic Size Dependence in the Hole Mobility of Methoxide-Stabilized PbSe Quantum Dot Solids. *ACS Nano* **7**, 2013, 6774–6781.

[28] Wolcott, A.; Doyeux, V.; Nelson, C. A.; Gearba, R.; Lei, K. W.; Yager, K. G.; Dolocan, A. D.; Williams, K.; Nguyen, D.; Zhu, X.-Y. Anomalously Large Polarization Effect Responsible for Excitonic Red Shifts in PbSe Quantum Dot Solids. *J. Phys. Chem. Lett.* **2**, 2011, 795–800.

[29] Banin, U.; Cao, Y.; Katz, D.; Millo, O. Identification of Atomic-like Electronic States in Indium Arsenide Nanocrystal Quantum Dots. *Nature* **400**, 1999, 542–544.

[30] Overgaag, K.; Liljeroth, P.; Grandidier, B.; Vanmaekelbergh, D. Scanning Tunneling Spectroscopy of Individual PbSe Quantum Dots and Molecular Aggregates Stabilized in an Inert Nanocrystal Matrix. *ACS Nano* **2**, 2008, 600–606.

[31] Wolf, O.; Dasog, M.; Yang, Z.; Balberg, I.; Veinot, J. G. C.; Millo, O. Doping and Quantum Confinement Effects in Single Si Nanocrystals Observed by Scanning Tunneling Spectroscopy. *Nano Lett.* **13**, 2013, 2516–2521.

[32] Kaushik, A. P.; Lukose, B.; Clancy, P. The Role of Shape on Electronic Structure and Charge Transport in Faceted PbSe Nanocrystals. *ACS Nano* 2014, DOI: 10.1021/nn405755n.

[33] Hoffmann, R. Small but Strong Lessons from Chemistry for Nanoscience. *Angew. Chem. Int. Ed.* **52**, 2013, 93–103.

[34] Lauth, J.; Marbach, J.; Meyer, A.; Dogan, S.; Klinke, C.; Kornowski, A.; Weller, H. Virtually Bare Nanocrystal Surfaces: Significantly Enhanced Electrical Transport in $CuInSe_2$ and $CuIn_{1-x}Ga_xSe_2$ Thin Films Upon Ligand Exchange with Thermally Degradable 1-Ethyl-5-Thiotetrazole. *Adv. Funct. Mater.* **24**, 2014, 1081–1088.

[35] Huynh, W. U.; Dittmer, J. J.; Alivisatos, A. P. Hybrid Nanorod-Polymer Solar Cells. *Science* **295**, 2002, 2425–2427.

[36] Agranovich, V. M.; Gartstein, Y. N.; Litinskaya, M. Hybrid Resonant Organic-Inorganic Nanostructures for Optoelectronic Applications. *Chem. Rev.* **111**, 2011, 5179–5214.

[37] Kim, Y.; Song, N. W.; Yu, H.; Moon, D. W.; Lim, S. J.; Kim, W.; Yoon, H.-J.; Koo Shin, S. Ligand-dependent Blinking of Zinc-blende CdSe/ZnS Core/shell Nanocrystals. *Phys. Chem. Chem. Phys.* **11**, 2009, 3497–3502.

[38] Cordones, A. A.; Scheele, M.; Alivisatos, A. P.; Leone, S. R. Probing the Interaction of Single Nanocrystals with Inorganic Capping Ligands: Time-Resolved Fluorescence from CdSe-CdS Quantum Dots Capped with Chalcogenidometalates. *J. Am. Chem. Soc.* **134**, 2012, 18366–18373.

[39] Cordones, A. A.; Bixby, T. J.; Leone, S. R. Direct Measurement of Off-State Trapping Rate Fluctuations in Single Quantum Dot Fluorescence. *Nano Lett.* **11**, 2011, 3366–3369.

[40] Zhang, J. Z.; Ellis, A. B. Adsorption of TCNQ Derivatives onto the Surface of Cadmium Selenide Single Crystals: Quenching of Semiconductor Photoluminescence by a Family of Strong .pi-acids. *J. Phys. Chem.* **96**, 1992, 2700–2704.

[41] Frederick, M. T.; Amin, V. A.; Swenson, N. K.; Ho, A. Y.; Weiss, E. A. Control of Exciton Confinement in Quantum Dot-Organic Complexes through Energetic Alignment of Interfacial Orbitals. *Nano Lett.* **13**, 2012, 287–292.

[42] Frederick, M. T.; Amin, V. A.; Weiss, E. A. Optical Properties of Strongly Coupled Quantum Dot-Ligand Systems. *J. Phys. Chem. Lett.* **4**, 2013, 634–640.

[43] Wessels, J. M.; Nothofer, H.-G.; Ford, W. E.; Wrochem, F. von; Scholz, F.; Vossmeyer, T.; Schroedter, A.; Weller, H.; Yasuda, A. Optical and Electrical Properties of Three-Dimensional Interlinked Gold Nanoparticle Assemblies. *J. Am. Chem. Soc.* **126**, 2004, 3349–3356.

[44] Guyot-Sionnest, P. Electrical Transport in Colloidal Quantum Dot Films. *J. Phys. Chem. Lett.* **3**, 2012, 1169–1175.

[45] Bendikov, M.; Wudl, F.; Perepichka, D. F. Tetrathiafulvalenes, Oligoacenenes, and Their Buckminsterfullerene Derivatives: The Brick and Mortar of Organic Electronics. *Chem. Rev.* **104**, 2004, 4891–4946.

[46] Hyun, B.-R.; Zhong, Y.-W.; Bartnik, A. C.; Sun, L.; Abruna, H. D.; Wise, F. W.; Goodreau, J. D.; Matthews, J. R.; Leslie, T. M.; Borrelli, N. F. Electron Injection from Colloidal PbS Quantum Dots into Titanium Dioxide Nanoparticles. *ACS Nano* **2**, 2008, 2206–2212.

[47] Jasieniak, J.; Califano, M.; Watkins, S. E. Size-Dependent Valence and Conduction Band-Edge Energies of Semiconductor Nanocrystals. *ACS Nano* **5**, 2011, 5888–5902.

[48] Axnanda, S.; Scheele, M.; Crumlin, E.; Mao, B.; Chang, R.; Rani, S.; Faiz, M.; Wang, S.; Alivisatos, A. P.; Liu, Z. Direct Work Function Measurement by Gas Phase Photoelectron Spectroscopy and Its Application on PbS Nanoparticles. *Nano Lett.* **13**, 2013, 6176–6182.

[49] Heimel, G.; Duhm, S.; Salzmann, I.; Gerlach, A.; A., S.; Niederhausen, J.; Bürker, C.; Hosokai, T.; Fernandez-Torrente, I.; Schulze, G.; *et al.* Charged and Metallic Molecular Monolayers through Surface-induced Aromatic Stabilization. *Nat Chem* **5**, 2013, 187–194.

[50] Nordin, M. N.; Bourdakos, K. N.; Curry, R. J. Charge Transfer in Hybrid Organic-inorganic PbS Nanocrystal Systems. *Phys. Chem. Chem. Phys.* **12**, 2010, 7371–7377.

[51] Shevchenko, E. V.; Talapin, D. V.; Kotov, N. A.; O'Brien, S.; Murray, C. B. Structural Diversity in Binary Nanoparticle Superlattices. *Nature* **439**, 2006, 55–59.

[52] Luther, J. M.; Law, M.; Song, Q.; Perkins, C. L.; Beard, M. C.; Nozik, A. J. Structural, Optical, and Electrical Properties of Self-Assembled Films of PbSe Nanocrystals Treated with 1,2-Ethanedithiol. *ACS Nano* **2**, 2008, 271–280.

[53] Zarghami, M. H.; Liu, Y.; Gibbs, M.; Gebremichael, E.; Webster, C.; Law, M. p-Type PbSe and PbS Quantum Dot Solids Prepared with Short-Chain Acids and Diacids. *ACS Nano* **4**, 2010, 2475–2485.

[54] Wang, Z.; Schliehe, C.; Bian, K.; Dale, D.; Bassett, W. A.; Hanrath, T.; Klinke, C.; Weller, H. Correlating Superlattice Polymorphs to Internanoparticle Distance, Packing Density, and Surface Lattice in Assemblies of PbS Nanoparticles. *Nano Lett.* **13**, 2013, 1303–1311.

[55] Scheele, M.; Hanifi, D.; Zherebetskyy, D.; Chourou, S. T.; Axnanda, S.; Rancatore, B. J.; Thorkelsson, K.; Xu, T.; Liu, Z.; Wang, L.-W.; *et al.* PbS Nanoparticles Capped with Tetrathiafulvalene-tetracarboxylate: Utilizing Energy Level Alignment for Efficient Carrier Transport. *ACS Nano* **8**, 2014, 2532–2540.